NEOPLASIA
www.neoplasia.com

Volume 11 Number 11 November 2009 pp. 1132–1145 **1132**

Adenosine A_3 Receptor Suppresses Prostate Cancer Metastasis by Inhibiting NADPH Oxidase Activity[1,2]

Sarvesh Jajoo*,[3], Debashree Mukherjea*,[3], Kounosuke Watabe† and Vickram Ramkumar*

*Department of Pharmacology, Southern Illinois University School of Medicine, Springfield, IL 62794, USA; †Department of Medical Microbiology, Immunology and Cell Biology, Southern Illinois University School of Medicine, Springfield, IL 62794, USA

Abstract

Prostate cancer is the most commonly diagnosed and second most lethal malignancy in men, due mainly to a lack of effective treatment for the metastatic disease. A number of recent studies have shown that activation of the purine nucleoside receptor, adenosine A_3 receptor (A_3AR), attenuates proliferation of melanoma, colon, and prostate cancer cells. In the present study, we determined whether activation of the A_3AR reduces the ability of prostate cancer cells to migrate *in vitro* and metastasize *in vivo*. Using severe combined immunodeficient mice, we show that proliferation and metastasis of AT6.1 rat prostate cancer cells were decreased by the administration of A_3AR agonist N^6-(3-iodobenzyl) adenosine-5′-*N*-methyluronamide. *In vitro* studies show that activation of A_3AR decreased high basal nicotinamide adenine dinucleotide phosphate (NADPH) oxidase activity present in these cells, along with the expression of Rac1 and $p47^{phox}$ subunits of this enzyme. Inhibition of NADPH oxidase activity by the dominant-negative RacN17 or short interfering (si)RNA against $p47^{phox}$ reduced both the generation of reactive oxygen species and the invasion of these cells on Matrigel. In addition, we show that membrane association of $p47^{phox}$ and activation of NADPH oxidase is dependent on the activity of the extracellular signal–regulated kinase (ERK)1/2 mitogen-activated protein kinase pathway. We also provide evidence that A_3AR inhibits ERK1/2 activity in prostate cancer cells through inhibition of adenylyl cyclase and protein kinase A. We conclude that activation of the A_3AR in prostate cancer cells reduces protein kinase A–mediated stimulation of ERK1/2, leading to reduced NADPH oxidase activity and cancer cell invasiveness.

Neoplasia (2009) 11, 1132–1145

Introduction

In the United States, the number of new cases and deaths due to prostate cancer were estimated at 186,320 and 28,660, respectively, for the year 2008 [1]. The major cause of deaths is due to the complications resulting from cancer metastases to distant organs in the body. The 5-year survival rate for the localized disease is close to 90% to 100%, but it is just approximately 32% for the metastatic prostate cancer [1], reflecting the lack of effective treatment for the metastatic disease, associated with androgen insensitivity.

Cancer cell metastasis requires the cell to acquire an early motile phenotype followed by transformation to an adhesive phenotype to facilitate interaction with the extracellular matrix proteins. This allows for dispersion of the malignant cells through the blood stream or lymph vessels to other parts of the body [2]. The Rho family of small GTP binding proteins, namely, Rac1 and Cdc42, play crucial roles in cancer cell metastasis [3]. Aberrant activation of these proteins promotes

Abbreviations: A_3AR, adenosine A_3 receptor; AEBSF, 4-(2-aminoethyl)benzenesulfonyl fluoride hydrochloride; DPI, dibenziodolium chloride; ERK1/2, extracellular signal–regulated kinase 1/2; H-89, *N*-[2-(*p*-bromocinnamylamino)ethyl]-5-isoquinolinesulfonamide dihydrochloride; H_2DCFDA, 2′,7′-dichlorodihydrofluorescein diacetate; IB-MECA, N^6-(3-iodobenzyl)adenosine-5′-*N*-methyluronamide; MRS1523, 3-propyl-6-ethyl-5-[(ethylthio)carbonyl]-2 phenyl-4-propyl-3-pyridine carboxylate; NADPH oxidase, nicotinamide adenine dinucleotide phosphate oxidase; PD098059, 2-(2-amino-3-methoxyphenyl)-4*H*-1-benzopyran-4-one; ROS, reactive oxygen species; siRNA, short interfering RNA; SQ22536, 9-(tetrahydro-2-furanyl)-adenine

Address all correspondence to: Vickram Ramkumar, PhD, PO Box 19629, SIU School of Medicine, Springfield, IL 62794. E-mail: vramkumar@siumed.edu

[1]This research was supported by NIH Grant (R15CA135494), SIU School of Medicine Cancer Center Grant and SIU School of Medicine Excellence in Academic Medicine Award to V.R. and Department of Defense Grant (W81XWH-07-1-0202) and NIH Grant (R01CA124650) to K.W.

[2]This article refers to supplementary materials, which are designated by Figures W1 to W6 and are available online at www.neoplasia.com.

[3]These authors contributed equally to the completion of this study.

Received 8 May 2009; Revised 11 July 2009; Accepted 13 July 2009

Copyright © 2009 Neoplasia Press, Inc. All rights reserved 1522-8002/09/$25.00
DOI 10.1593/neo.09744

invasion of various cancers [4–6] through regulation of actin cytoskeletal structures [7].

In addition to its role in cell motility, Rac1 is also an essential component of the nicotinamide adenine dinucleotide phosphate (NADPH) oxidase system, a major source of superoxide generation in the cell. NADPH oxidase was initially thought to be expressed mainly in phagocytes where it contributes to killing of ingested microorganisms through the generation of superoxide [8]. However, NADPH oxidase subunits are also expressed in other tissues [9]. Full enzyme activity is conferred by four oxidase subunits, namely, $gp91^{phox}$, $p22^{phox}$, $p47^{phox}$, and $p67^{phox}$ [10]. Other proteins associated with activation of the holoenzyme include $p40^{phox}$, Rap1A, and Rac1, whose activation promotes NADPH oxidase activity and generation of reactive oxygen species (ROS) [10].

Whereas it is known that ROS increase oncogenic transformation by damaging DNA and increasing mutation rates, recent evidence demonstrates that ROS activate cell signaling pathways to promote proliferation and metastasis [11]. ROS act as signaling molecules of growth factor receptors to activate mitogen-activated protein (MAP) kinases such as p38, extracellular signal–regulated kinase (ERK), and c-Jun N-terminal kinase [12]. These signaling pathways culminate in the regulation of cell cycle proteins, thereby influencing the proliferation of cancer cells. In the context of growth factor signaling, NADPH oxidase plays a key role in generating ROS [10].

Adenosine-based drugs represent a novel class of compounds that show antitumor effects against a number of different cancers. Four major classes of adenosine receptors (ARs), namely, the A_1, the A_{2A}, A_{2B}, and A_3AR [13], have been identified. Adenosine and different AR agonists have been shown to affect the tumorigenicity of different cancer types. A_1AR agonists inhibit the proliferation of various cancer cell lines including epidermoid cancer cells [14] and human leukemia cells [15], whereas activation of the A_{2B}AR increased tumor growth [16]. Recent studies have shown an antitumorigenic action of A_3AR agonists against melanoma [17], colon [18], and prostate cancers [19]. The mechanism underlying this action involves inhibition of cyclic AMP production, leading to reduced protein kinase A (PKA) and glycogen synthase kinase-3β activity, destabilization of β-catenin and suppression of cyclin D1 and *c-myc*, cell cycle arrest, and/or apoptosis [20,21]. A_3AR agonists were also shown to increase migration of human colon cancer cells [22]. However, this observation was obtained in *in vitro* hypoxic culture conditions. Induction of the A_3AR occurs in several types of cancer [21,23], when compared with normal adjacent tissue, suggesting that these receptors could serve as potential molecular markers of these cancers.

In this study, we show that the A_3AR agonist, IB-MECA, inhibits *in vivo* tumor growth and metastasis of prostate cancer in mice, in addition to inhibition of *in vitro* cell proliferation and invasion of prostate cancer cells. This antitumor action involves suppression of high ROS generation through the NADPH oxidase system, which is maintained through high ERK1/2 activity in these cells. We show that A_3AR suppresses ERK1/2 and NADPH oxidase activity by inhibiting a cyclic AMP/PKA pathway in these cells.

Materials and Methods

Materials

N^6-(3-Iodobenzyl)adenosine-5′-*N*-methyluronamide (IB-MECA), 3-propyl-6-ethyl-5-[(ethylthio)carbonyl]-2 phenyl-4-propyl-3-pyridine carboxylate (MRS1523), 4-(2-aminoethyl)benzenesulfonyl fluoride hydrochloride (AEBSF), dibenziodolium chloride (DPI), 2-(2-amino-3-methoxyphenyl)-4*H*-1-benzopyran-4-one (PD098059), 9-(tetrahydro-2-furanyl)-adenine (SQ22536), *N*-[2-(*p*-bromocinnamylamino) ethyl]-5-isoquinolinesulfonamide dihydrochloride (H-89), and bisindolylmaleimide I hydrochloride (BIM) were obtained from Sigma Chemical, Co (St Louis, MO). Antibodies against adenosine A_3 receptor (A_3AR), phospho-ERK1/2, ERK1/2, $p47^{phox}$ Rac1, and Na^+-K^+ ATPase were purchased from Santa Cruz Biotechnology, Inc (Santa Cruz, CA). Antibodies against β-actin and against Bax and p53 were bought from Sigma Chemical, Co, and Cell Signaling Technology (Danvers, MA), respectively. Cell culture media RPMI 1640 and penicillin/streptomycin were obtained from Invitrogen (Carlsbad, CA), whereas fetal bovine serum was from Atlanta Biologicals, Inc (Lawrenceville, GA). All other reagents and supplies were of highest available grade and were purchased from standard sources.

Cell Cultures

The rat prostatic carcinoma cell line AT6.1, and human prostate cancer cell lines ALVA and PC3-MM were cultured in RPMI 1640 media supplemented with 10% fetal bovine serum, 50 U/ml penicillin, and 25 μg/ml streptomycin. Cells were grown at 37°C in the presence of 5% CO_2 and 95% ambient air. The medium was changed every second day, and the cells were passaged twice a week. All the experiments were performed using confluent monolayers.

Immunocytochemistry

AT6.1, PC3-MM, or ALVA cells were cultured on glass coverslips. Drug treatments were performed for 24 hours, and cells were fixed with 4% paraformaldehyde. Cells were processed and imaged for A_3AR and Rac1 as described previously [24].

2′,7′-Dichlorodihydrofluorescein Diacetate Assay

After 12 hours of serum deprivation AT6.1, PC3-MM, or ALVA cells were loaded with 5 μg/ml of 2′,7′-dichlorodihydrofluorescein diacetate (H_2DCFDA; EMD Biosciences, San Diego, CA) in 2 ml of 1× PBS. After incubation at 37°C for 20 minutes, cells were washed with 1× PBS. First, baseline images were recorded by a confocal microscope (Olympus America, Inc, Melville, NY) at 488 nm, and then the image was captured after the addition of 1 μM IB-MECA. For other treatment groups, cells were pretreated with either vehicle or A_3AR inhibitor MRS 1523 (1 μM) or NADPH oxidase inhibitors DPI (10 μM) or AEBSF (100 μM) for 30 minutes before adding the dye. Quantitation of the fluorescence intensity was performed by using FluoView software (Olympus America, Inc, Melville, NY).

Preparation of Plasma Membrane and Cytosolic Extracts

Cytosolic and membrane extracts from whole cell lysates were isolated as described previously [24]. To verify the purity of the membrane isolates, we probed for the membrane-specific protein Na^+-K^+ ATPase. High Na^+-K^+ ATPase levels were obtained in the membrane fraction by Western blot analysis compared with the cytosol (data not shown).

Western Blot Analysis

Total cell lysates were used to quantitate activation/inhibition of ERK1/2 and expression of Rac1, whereas membrane preparations were made to study the expression of A_3AR. Assays were performed essentially as described previously [24]. Blots were visualized by

exposure to Kodak XAR film (Fisher Scientific, Pittsburgh, PA) or by using a charge-coupled device camera (Hitachi Genetic Systems, MiraiBio, Inc, Alameda, CA). Quantitation of the bands was performed with Un-Scan-It software (Silk Scientific, Inc, Orem, UT).

Transient Transfection of AT6.1 Cells

AT6.1 cells (2.0×10^5/ml) were seeded on coverslips in six-well culture plates and grown to 70% confluence. A mixture of 1 μg of plasmid DNA from vectors expressing constitutively active Rac (RacQL) or dominant-negative Rac (RacN17) was used, and transfections with ExGen500 were performed as described previously [25].

In Vitro *Invasion Chamber Assay*

The ability of prostate cancer cells to migrate through Matrigel-coated membranes was measured using BD Biocoat Matrigel invasion chambers (BD Biosciences, San Jose, CA). AT6.1, PC3-MM, and ALVA cells (200,000 cells) were suspended in the culture media without serum and were plated on the top compartment of the invasion chamber followed by respective treatments. At the end of 24 hours, the cell inserts were removed, and cells were carefully wiped from the top surface of the membrane with a cotton swab. The invasive cells adhering to the bottom surface of the membrane were stained with toluidine blue and quantified under a light microscope using a 20× objective. Total number of invaded cells was counted in eight randomly chosen fields per treatment per insert. To study the effects of the short interfering RNA (siRNA)–p47 and Rac1 plasmids, AT6.1 cells were transfected with siRNA-p47 and siRNA-negative for 72 hours or with empty vector or constitutively active (RacQL) or dominant-negative (RacN17) plasmids for 12 hours before seeding them on the top compartment.

Cell Proliferation Assay (MTS Assay)

In vitro prostate cancer cell proliferation was performed by using CellTiter 96 AQ_{ueous} One Solution Cell Proliferation Assay Kit (Promega, Madison, WI), according to the manufacturer's instructions. In brief, 1 to 3×10^3 cells per well were seeded into a 96-well plate. After respective treatments, cells were allowed to grow for 72 hours. After 72 hours, 20 μl of CellTiter 96 AQ_{ueous} One Solution reagent was added to each well in 100 μl of total volume. Cells were incubated for 3 to 4 hours, and absorbance was recorded at 490 nm using a plate reader.

Apoptosis Detection

For detecting apoptosis in AT6.1 cells, apoptotic cells were visualized using fluorimetric TdT-FragEL DNA fragmentation detection kit performed according to the manufacturer's instructions (EMD Biosciences). Briefly, the cells were treated with vehicle, IB-MECA, or positive control for 24 hours. After the treatments, the cells were washed with cold 1× PBS and fixed with 4% paraformaldehyde. Fixed cells were permeabilized with 20 μg/ml of proteinase K for 5 minutes, washed with 1× TBS, and placed in 1× TdT equilibrating buffer for 20 minutes. Cells were then incubated in labeling reaction buffer containing Fluorescein-FragEL TdT labeling reaction mix and TdT enzyme for 60 minutes at 37°C in a humidified chamber. After one wash with 1× TBS and 10 minutes of incubation in blocking buffer, cells were mounted on glass slide and visualized by confocal microscope. Apoptotic cells were identified as those emitting bright green fluorescence, whereas control/nonapoptotic cells were either nonfluorescent or faintly green fluorescent.

Cyclic AMP Assay

Cyclic AMP levels were measured with a chemiluminescence-based cyclic AMP HTS immunoassay kit from Millipore (Billerica, MA) according to the manufacturer's instructions.

Modified Wound-Healing Assay

Equal number of cells were plated in each well of six-well culture plates. After the cells reached 70% to 80% confluence, one half of the well was denuded by scraping off the cells with a cell scraper. The images were recorded before and just after the denudation (time, 0 hours). Cells were then treated with different reagents and incubated for another 24 hours, and differential interference contrast (DIC) images of the cells were captured by confocal microscopy. For quantitation, cells were counted in five random fields in the marked area and normalized to vehicle-treated controls.

In Vivo *Studies*

To determine the spontaneous metastatic ability of the AT6.1 prostate tumor cells, 0.5×10^6 cells in 0.2 ml of 1× PBS were injected intravenously through the tail vein of 5-week-old severe combined immunodeficient (SCID) mice with an average weight of 20 g (Harlan Sprague-Dawley, Indianapolis, IN). Mice were divided into two treatment groups, namely, control and IB-MECA groups, and treatments were started at the same time of tumor cell injections. Control mice were treated with 200 μl of vehicle (dH_2O), whereas IB-MECA–treated mice received 10 μg/kg of IB-MECA in a final volume of 200 μl. Vehicle or drug was administered on alternate days by intraperitoneal (i.p.) injections. Mice were killed 3 weeks after the injection of the cells, and metastatic lesions on the lungs were counted macroscopically. For effects on tumor growth, drug administration was performed as described above, but the tumor cells were inoculated subcutaneously in the dorsal flank of the mice, and treatments were started after 9 days when the tumor size reached 100 mm^3. The tumor sizes were measured twice a week with a caliper, and the tumor volume was calculated using the formula, tumor volume = $(W^2) \times (L / 2)$, where W represents the width and L represents the tumor length. The tumor size was measured until day 33 after tumor inoculation, after which the mice were killed, and tumors were removed and flash-frozen for Western blot studies. In the same group of mice, a number of metastatic lesions were counted on the lungs to measure the effect of IB-MECA on the metastatic ability of AT6.1 cells after subcutaneous inoculation of tumor cells.

siRNA Transfections

siRNA transfections were done using RNAi human/mouse starter kit from Qiagen (Valencia, CA) according to the manufacturer's protocol. Briefly, 3 to 4×10^5 AT6.1 cells were plated. Next day, different concentrations (0-50 nM) of $p47^{phox}$ siRNA were diluted in 100-μl serum-free medium and were incubated at room temperature for 5 to 10 minutes with 3 μl of HiPerFect transfection reagent (Qiagen) to allow the formation of transfection complexes, which were added to the cell cultures by gently swirling the plates. Cells were incubated for another 72 hours and later used for quantitating $p47^{phox}$ by Western blot analysis. For all other subsequent experiments, the same protocol was used with 50 nM $p47^{phox}$ siRNA.

RNA Preparation, Reverse Transcription, and Polymerase Chain Reaction

Isolation of total RNA from cells was performed by using Tri reagent (Sigma Chemical, Co), as directed by the manufacturer. The respective products were normalized to glyceraldehyde-3-phosphate dehydrogenase (GAPDH).

Real-time Reverse Transcription–Polymerase Chain Reaction

Total RNA was isolated and converted to complementary DNA using iScript cDNA Synthesis Kit (Bio-Rad Laboratories, Hercules, CA), and quantitative reverse transcription–polymerase chain reaction (RT-PCR) was performed as described previously [25]. The PCR products were resolved on 2% agarose gel and viewed with SyBRGreen dye. Gel intensity analysis was performed by using Un-Scan-It software.

PCR Primers

The set of primer sequences were from Sigma Genosys (St Louis, MO).

A_3AR:
5′-CATCTGGGTGGTCAAGCTGAA-3′ (sense);
5′-ACCGTTCTATATCTGACTGTC-3′ (antisense).
Rac1:
5′-ATCAGTTACACGACCAATGC-3′ (sense);
5′-GGGAAAAGCAAATTAAGAAC-3′ (antisense).
$p47^{phox}$:
5′-CATGTTCCTGGTTAAGTGGCA-3′ (sense);
5′-AGGTGTGGGCAGCGGGAGATC-3′ (antisense).
GAPDH:
5′-ATGGTGAAGGTCGGTGTGAAC-3′ (sense);
5′-TGTAGTTGAGGTCAATGAAGG-3′ (antisense).

Protein Determination

The levels of protein in samples were determined by Bio-Rad protein detection reagent using bovine serum albumin to prepare standard curves.

Statistical Analyses

Statistical analyses were performed by using analysis of variance followed by Tukey's honestly significant difference *post hoc* test to compensate for multiple pairwise comparisons or by paired Student's *t* test.

Results

A_3AR Agonist IB-MECA Inhibits Proliferation and Invasion of Prostate Cancer Cells

To study the effects of A_3AR on tumor cell growth and invasion, we performed *in vitro* studies using the androgen-independent metastatic human prostate carcinoma cells (PC3-MM), the androgen-dependent human prostate carcinoma cells (ALVA), and the androgen-independent highly metastatic rat prostate carcinoma cells (AT6.1). These cell lines expressed A_3AR, as demonstrated in Figure 1*A* by RT-PCR (*top left*), Western blot analysis (*top right*), and immunocytochemistry (*bottom*). To determine whether A_3AR activation inhibits proliferation of prostate cancer cells, MTS assays were performed in the presence of IB-MECA (1 μM), an agonist of the A_3AR, with or without the selective antagonist MRS1523 (1 μM). Figure 1*B* demonstrates that exposure to IB-MECA for 72 hours led to significant reductions in proliferation of these cells to 59 ± 2%, 50 ± 6%, and 64 ± 3% of vehicle-treated controls for PC3-MM, ALVA, and AT6.1 cells, respectively. This antiproliferative response was reduced by MRS1523; the respective proliferative indices in these lines were 98 ± 7%, 111 ± 14%, and 96 ± 6% of vehicle-treated controls (Figure 1*B*). We did not obtain any significant inhibition of proliferation of these cells after exposure to IB-MECA for 24 hours. For AT6.1 cells, the cell numbers obtained after 24 hours of exposure to IB-MECA, MRS1523, and IB-MECA + MRS1523 were 89 ± 8%, 96 ± 9%, and 88 ± 7% of control.

To assess the effects of A_3AR activation on prostate cancer cell invasion and migration *in vitro*, we used Matrigel invasion chamber and wound-healing assays, respectively. Treatment with IB-MECA (1 μM) for 24 hours decreased the number of invaded cells, as seen by toluidine blue staining of the cells on Matrigel membrane, to 47 ± 3%, 49 ± 1%, and 38 ± 8% of vehicle-treated controls in PC3-MM, ALVA, and AT6.1 cell lines, respectively. This inhibition by IB-MECA was significantly reduced by MRS1523 (Figure 1*C*), implicating the A_3AR in this process. In addition, IB-MECA reduced the migration of AT6.1 cells, as demonstrated by reduced cell migration in wound-healing assays. IB-MECA decreased migration to 52 ± 2% of vehicle-treated controls, which was blocked by coadministration of IB-MECA with MRS1523 (Figure 1*D*). These data indicate that activation of the A_3AR suppresses both the proliferation and invasion/migration of prostate cancer cells *in vitro*. However, it seemed that these two processes are independent of each other because significant inhibition of invasion and migration was observed at 24 hours, a time point when no effect on cell proliferation was evident.

Cells exposed to IB-MECA for 24 hours did not show any increase in apoptotic cell death, as determined by TdT-FragEL DNA fragmentation assay in cells (Figure W1*A*). In addition, IB-MECA did not increase the levels of proapoptotic proteins Bax and p53 (Figure W1, *B* and *C*). These results further support the lack of inhibition of proliferation of prostate cancer lines obtained at 24 hours in MTS assays. Nevertheless, continued exposure to IB-MECA for 48 and 72 hours increased the levels of Bax and p53 (data not shown). These data suggest that the reduction in cell number obtained at 72 hours in the presence of IB-MECA could result, in part, from increased apoptosis.

IB-MECA Inhibits In Vivo *Prostate Tumor Growth and Metastasis*

To determine the relevance of our *in vitro* findings, we examined tumor growth and metastasis of AT6.1 prostate cancer cells in a SCID mouse model. AT6.1 cells were injected subcutaneously into the dorsal flank of SCID mice and when the tumor size was approximately 100 mm^3 (by approximately day 9), these mice were administered either vehicle or IB-MECA (10 μg/kg body weight, i.p.) on alternate days. Figure 2*A* shows a progressive increase in tumor volumes over time in mice administered vehicle but significantly reduced tumor sizes in mice administered IB-MECA. Tumor volumes measured on day 14 were 573 ± 57 mm^3 in vehicle-treated control mice and 276 ± 52 mm^3 after IB-MECA treatment ($n = 6$; $P < .01$). On days 23 and 33, tumor volumes were 2794 ± 142 and 6153 ± 721 mm^3, respectively, for the controls but were reduced to 1276 ± 127 and 2261 ± 646 mm^3 after IB-MECA treatments ($n = 6$; $P < .01$). Examination of the lungs from these animals indicates that subcutaneous injection of AT6.1 cells reduced lung metastasis. The number of lesions observed in vehicle-treated mice was 37 ± 8 and was significantly reduced to 12 ± 1 in mice treated with IB-MECA. These data indicate that IB-MECA could reduce both prostate tumor sizes and metastasis *in vivo*.

To exclude the possibility that the reduced tumor metastasis produced by IB-MECA after subcutaneous injections of tumor cells was

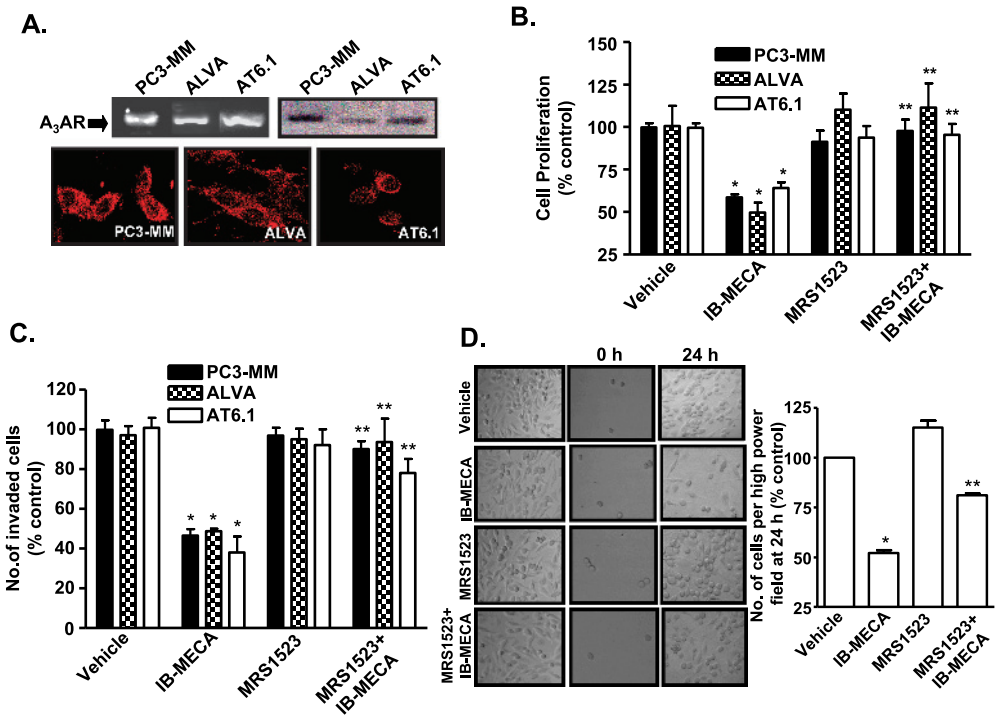

Figure 1. A_3AR agonist IB-MECA inhibits proliferation and invasion of different prostate cancer cell lines. (A) Expression of A_3AR in prostate cancer cell lines, PC3-MM, ALVA, and AT6.1, was determined by RT-PCR (top left), Western blot analysis (top right), and immunocytochemistry (bottom). The pictures shown are the representation of three different experiments with similar results. (B) PC3-MM, ALVA, and AT6.1 cells were plated in a 96-well plate and treated with vehicle or IB-MECA (1 μM) or MRS1523 (1 μM) or MRS1523 with IB-MECA for 72 hours. Cell proliferation was assessed by MTS assays. Values represented are mean ± SEM of four different experiments, each of which shows the average data obtained from 16-well per treatment group. Asterisk (*) indicates statistically significant difference ($P < 0.01$) from control, whereas (**) indicates statistically significant difference ($P < 0.01$) from IB-MECA–treated cells. (C) Cells were plated on the top chamber of the Matrigel invasion chamber. Treatments were performed for 24 hours and numbers of invaded cells were counted on the membranes stained with toluidine blue. Numbers depicted in histogram are mean ± SEM of three separate experiments, each performed with duplicate chambers per treatment group. Asterisks (*) and (**) indicate statistically significant difference ($P < .05$) from control and IB-MECA treatment groups, respectively. (D) AT6.1 cells migration in cultures was assessed by modified wound-healing assays in which at 70% to 80% confluence, half of cell cultures were denuded by scraping the cells with a cell scraper at time 0 hours. The cells were imaged (middle panel) and treated with vehicle or IB-MECA (1 μM) or MRS1523 (1 μM) or MRS1523 + IB-MECA for 24 hours. After 24 hours, DIC images were obtained of the marked denuded area. Five random fields were chosen for images (right panel), and numbers of cells were counted per field and were represented in the bar graph as the mean ± SEM of three different experiments. Asterisks (*) and (**) indicate statistically significant difference ($P < .05$) from vehicle-treated control and IB-MECA treated cells, respectively.

independent of its action on proliferation, we induced experimental tumor metastasis by injecting AT6.1 cells intravenously through the tail vein. IB-MECA (10 μg/kg body weight, i.p.) was administered at the time of cell administration and on alternate days for 3 weeks. Mice were then killed, lungs were isolated, and metastatic lesions were counted macroscopically. As shown in Figure 2*B*, this method of administration of the prostate cancer cells dramatically increased the number of metastatic lesions in the lung. Administration of IB-MECA significantly reduced the number of metastatic lesions in the lungs from 208 ± 18 in vehicle-treated mice to 89 ± 29 by IB-MECA–treated mice (Figure 2*C*). These data support the finding that IB-MECA inhibits prostate cancer metastasis *in vivo* by blocking extravasation of cells to the lung.

A_3AR Agonist Reduces High ROS Generation in Prostate Cancer Cells by Inhibiting NADPH Oxidase

ROS plays an important role in oncogenesis by regulating genes involved in proliferation and metastasis of cells [11], which could account for the metastatic phenotype of tumor cells. To test whether IB-MECA alters ROS generation in these cells, we assessed its production using H_2DCFDA. AT6.1 cells showed high basal ROS levels, and incubation of cells with IB-MECA (1 μM) produced a rapid, time-dependent reduction in ROS generation, as demonstrated by the reduction in the green fluorescence (Figure 3*A*). Similar results were obtained with IB-MECA in ALVA and PC3-MM cells (Figure W2). The inhibition by IB-MECA was blocked in cells pretreated with 1 μM MRS1523 (Figure 3*A*), implicating the A_3AR in this process. ROS generation was 41 ± 5% of vehicle-treated controls in the presence of IB-MECA and 82 ± 8% in cells pretreated with MRS1523 before IB-MECA administration (Figure 3*B*). In addition, inhibition of NADPH oxidase with 10 μM DPI and 100 μM AEBSF effectively reduced ROS generation in these cells to 37 ± 9% and 45 ± 8% of control, respectively (Figure 3, *C* and *D*). However, inhibition of xanthine oxidase or nitric oxide synthase with allopurinol or *N*-nitro-L-arginine methyl ester (L-NAME), respectively, did not alter the level of ROS observed in these cells (data not shown). These results implicate NADPH oxidase in the generation of high ROS in these cells, which was inhibited by IB-MECA and NADPH oxidase inhibitors.

To confirm a role of NADPH oxidase as a source of ROS generation in AT6.1 cells, we targeted $p47^{phox}$ and Rac1, subunits of this

enzyme, for inhibition. Knockdown of $p47^{phox}$ was produced by transfecting cells with siRNA (50 nM) for 72 hours. This concentration of $p47^{phox}$ siRNA was based on dose-response studies of siRNA on $p47^{phox}$ protein levels (Figure W3*A*), which showed significant suppression of $p47^{phox}$ by Western blot analysis at a concentration of 50 nM. Control cultures were administered a similar concentration of a scrambled siRNA (siRNA-neg) sequence and tested concurrently. We observed that knockdown of $p47^{phox}$ reduced the high ROS generation (Figure 4, *A* and *B*) with no further inhibition observed with IB-MECA administration (data not shown). $p47^{phox}$ siRNA reduced ROS generation to 33 ± 6% of control cells. To determine a role of Rac1 in the generation of ROS, cells were transiently transfected with an empty vector, a plasmid construct expressing the constitutively active (RacQL) or dominant-negative mutant (RacN17) forms of Rac1. Transfection efficiency using ExGen500 in these cells averaged approximately 80 ± 10%, similar to that observed previously [25]. To show the levels of Rac1 expression in the cells transfected with the mutant plasmids, we performed RT-PCR and immunocytochemistry on the cells 24 hours after transfections. Increased Rac1 mRNA was detected in cells transfected with either RacQL or RacN17 plasmids, compared with cells transfected with the empty vector (Figure W3*B*). The levels of Rac1 mRNA detected were 160 ± 8% and 160 ± 11% of empty vector, for RacQL and RacN17 transfectants, respectively. In addition, increased Rac1 immunolabeling was detected in cells RacQL and RacN17 transfectants, compared with empty vector (Figure W3*C*). Higher immunolabeling for Rac1 was observed in the RacN17-transfected group (approximately 85% of cells per high-power field) and RacQL (approximately 92% of cells per high-power field) compared with empty vector (approximately 50% of cells per high-power field).

AT6.1 cells expressing the empty vector or RacQL demonstrated high ROS generation, whereas the cells transfected with RacN17 plasmid showed significantly lower levels of ROS generation (Figure 4, *D* and *E*). IB-MECA failed to inhibit the ROS generation in the presence of constitutively active RacQL (data not shown), suggesting that its action is mediated through inhibition of an upstream regulator of Rac1 function.

We next examined the role of ROS generation through NADPH oxidase in AT6.1 cell invasion. Knockdown of $p47^{phox}$ or inhibition of Rac1 (as previously mentioned) significantly reduced the invasion of AT6.1 cells compared with cells treated with a scrambled siRNA sequence (siRNA-Neg) or untransfected cells (vehicle; Figure 4, *C* and *F*). The numbers of invaded cells were 53 ± 3% and 35 ± 3% of control, in the presence of $p47^{phox}$ siRNA and RacN17, respectively. Interestingly, the expression of RacQL did not alter the level of invasion above that observed for the control cells, likely indicating that Rac1 is already maximally active in these cells. From these data, we conclude that NADPH oxidase plays a crucial role in regulation of ROS generation, which regulate the metastatic phenotype of AT6.1 cells.

IB-MECA Inhibits Activation and Expression of NADPH Oxidase Subunits

The inactive form of the $p47^{phox}$ subunit of NADPH oxidase resides in cytoplasm, which on activation by phosphorylation, translocates to the plasma membrane where it interacts with other subunits to form the holoenzyme needed to generate superoxide [9]. Thus, the

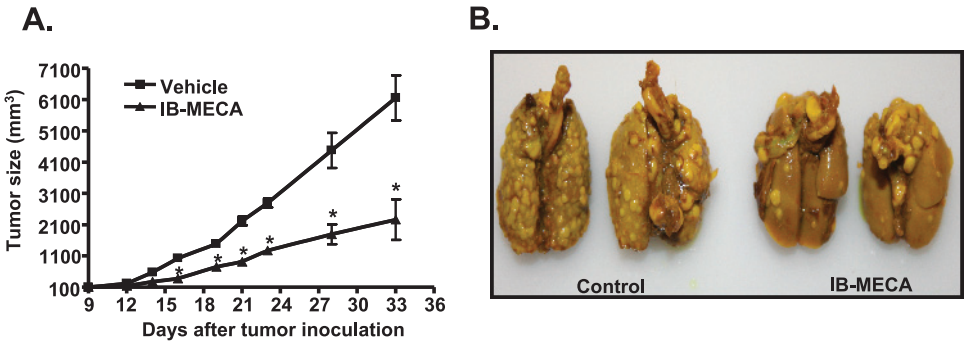

C.

Treatment groups	Total number of mice[a]	Lung metastases incidence[b]	Lung metastases (mean ± SEM)[c]	p value
Control	4	4/4	208 ± 18	
IB-MECA	4	4/4	89 ± 28	0.01

a. Number of SCID mice injected with AT6.1 tumor cells.
b. Number of SCID mice with lung metastases/number of SCID mice injected with tumor cells.
c. Number of lung metastatic lesions counted macroscopically per lung per SCID mouse.

Figure 2. IB-MECA suppresses prostate tumor growth and metastasis in mice. (A) Highly metastatic dunning rat prostate cancer (AT6.1) cells were injected subcutaneously in the dorsal flank of SCID mice. After 9 days, one group of mice was administered vehicle (control), whereas the other group was treated with 10 μg/kg IB-MECA (six mice per group). Tumor sizes were measured twice a week until day 33 of tumor inoculation. Asterisk (*) indicates statistically significant difference ($P < .01$) from control mice. (B) For experimental metastasis assays, mice were injected intravenously (through tail vein) with AT6.1 cells (four mice per group). Mice were treated with vehicle or IB-MECA on alternate days, starting from the day of cancer cell injection. After 3 weeks, mice were killed, and total numbers of metastatic lesions were counted in lungs. Representative pictures show lungs from two animals from each treatment group. (C) Summary of the effect of IB-MECA on lung metastases in SCID mice.

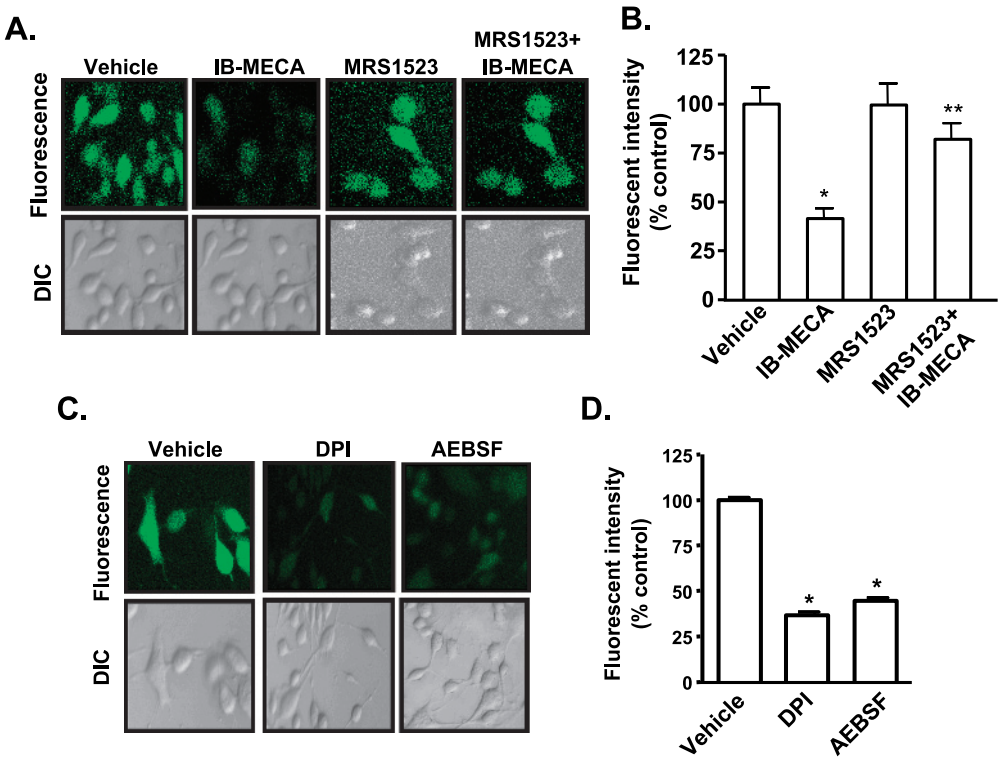

Figure 3. A_3AR mediated reduction of ROS generation in prostate cancer cells. (A and B) AT6.1 cells were pretreated for 30 minutes with either vehicle or 1 μM MRS1523 and then incubated with H_2DCFDA for 20 minutes. IB-MECA (1 μM) was added to the cells after recording baseline images, and subsequent images were recorded 15 minutes after addition of the drug with a confocal microscopy. Images shown are representative of four different experiments showing similar results. Quantitation of fluorescent images by FluoView software is presented in panel B. Similar experiments were performed in cells pretreated with 10 μM DPI or 100 μM AEBSF (C). Quantitation of fluorescent images from panel C is shown in panel D. Histograms represent the mean ± SEM of four different experiments. Asterisks (*) and (**) indicate statistically significant difference ($P < .05$) from vehicle and IB-MECA treatments, respectively.

degree of $p47^{phox}$ plasma membrane localization could serve as an indicator of NADPH oxidase activity in AT6.1 cells. Figure 5*A* shows high levels of $p47^{phox}$ in the plasma membrane compared with the cytosolic fraction in the absence of any drug treatments. However, IB-MECA decreased $p47^{phox}$ in the membrane fraction but increased cytosolic $p47^{phox}$ (Figure 5*A*). This effect of IB-MECA was inhibited by MRS1523, supporting a role of the A_3AR in decreasing $p47^{phox}$ translocation (Figure 5*B*). In addition, 24 hours of administration of IB-MECA reduced the steady-state expression of $p47^{phox}$ and Rac1 mRNA, with the respective mRNA levels being 0.5 ± 0.1- and 0.4 ± 0.1-fold of the control cells. Pretreatment with MRS1523 reversed the inhibition by IB-MECA, as demonstrated by $p47^{phox}$ and Rac1 mRNA levels of 1.1 ± 0.2- and 1.0 ± 0.1-fold of control in cells pretreated with MRS1523 followed by IB-MECA (Figure 5*C*). IB-MECA also inhibited expression of $p47^{phox}$ and Rac1 protein, as demonstrated in Figure 5, *D* and *E*, respectively. In the presence of 24 hours of IB-MECA treatment, the $p47^{phox}$ levels were 51 ± 9% of vehicle-treated controls, whereas they were 100 ± 14% in the cells pretreated with MRS1523 before IB-MECA treatment (Figure 5*D*). However, IB-MECA did not alter the expression of the $p22^{phox}$ and $p67^{phox}$ subunits of NADPH oxidase in AT6.1 cells but reduced the expression of the $gp91^{phox}$ homolog Nox1 (data not shown). These data indicate that the A_3AR inhibits both $p47^{phox}$ membrane localization and the expression of $p47^{phox}$ and Rac1.

Additional studies were performed to determine whether similar changes in $p47^{phox}$ and Rac1 could be induced *in vivo* by IB-MECA administration in SCID mice bearing AT6.1 subcutaneous tumors. AT6.1 cells were injected subcutaneously into the dorsal flank of SCID mice and IB-MECA treatment (10 μg/kg body weight, i.p.) was initiated when the tumor size was approximately 100 mm^3 (by day 9) and continued on alternate days until day 33. Subcutaneous tumors were excised and used for Western blot analysis. We observed a significant suppression of $p47^{phox}$ expression by IB-MECA in the primary tumor to 52 ± 13% of control (Figure 6, *A* and *B*). Similarly, Rac1 expression was reduced to 36 ± 6% of the expression level of vehicle-treated mice (Figure 6, *C* and *D*).

A_3AR Inhibition of $p47^{phox}$ Involves Inhibition of ERK1/2 MAP Kinase Activity

To determine the mechanism underlying IB-MECA inhibition of $p47^{phox}$ membrane localization, we focused on ERK1/2 MAP kinase signaling because this kinase mediates phosphorylation and activation of $p47^{phox}$ subunit in the immune system [26,27]. Inhibition of MAP kinase kinase, the immediate upstream activator of ERK1/2 by PD098059 (10 μM) reduced ROS generation to 42 ± 12% of control after a 15-minute treatment period (Figure 7*A*). PD098059 also altered the localization of $p47^{phox}$ in these cells. The levels of $p47^{phox}$ in membranes were 50 ± 14% and 57 ± 12% of controls after 5 and 15 minutes of PD098059 treatment, respectively (Figure 7*B*). There was a corresponding increase in cytosolic levels of $p47^{phox}$. After 5 and 15 minutes of treatment with PD098059, the cytosolic levels of $p47^{phox}$ were 167 ± 30% and 223 ± 39% of vehicle-treated cells (Figure 7*C*).

Because the preceding data suggest a potential role of ERK1/2 in regulating the activation of $p47^{phox}$ in AT6.1 cells, we next determined whether IB-MECA inhibits ERK1/2 activation in AT6.1 cells. As shown in Figure 7*D*, we observed high levels of p-ERK1/2 in AT6.1 cells, which were reduced to 31 ± 6% and 21 ± 5% of control levels by exposure to IB-MECA for 5 and 15 minutes, respectively, comparable to the effect of PD098059. This inhibitory effect of IB-MECA was dose-dependent (Figure W6) and was reduced by A_3AR antagonist MRS1523 (Figure 7*E*), implicating A_3AR activation in this process.

ERK1/2 activity was also regulated by high ROS because treatment of cells with DPI (10 μM) and AEBSF (100 μM) both reduced the p-ERK1/2 activation (Figure W4). These results suggest that whereas ERK1/2 is important for NADPH oxidase activity, the activity of ERK1/2 is also dependent on NADPH oxidase, implying the existence of a positive feedback loop between these two enzymes in these cells.

A_3AR Inhibition of ERK1/2 MAP Kinase Activity Is Mediated through Cyclic AMP/Protein Kinase A Pathway

The A_3AR is negatively coupled to adenylyl cyclase through the G_i protein, leading to a decrease in cyclic AMP levels and inhibition of PKA [28]. To determine whether A_3AR activation in AT6.1 cells regulates adenylyl cyclase activity, we determined cyclic AMP levels in cells treated with IB-MECA. Basal levels of cyclic AMP in these cells were 12.8 ± 0.6 pmol per well. Treatment of AT6.1 cells with IB-MECA significantly reduced the cyclic AMP generation to 6.3 ± 2.2 pmol per well ($n = 3$; $P < .05$). Pretreatment of cells with MRS1523 reversed the inhibition by IB-MECA to 12.6 ± 4.0 pmol per well (Figure W5), implicating the A_3AR in the inhibition of adenylyl cyclase.

To determine in more detail whether inhibition of the cyclic AMP pathway is important in mediating the antineoplastic actions of A_3AR activation, we examined the roles of adenylyl cyclase and PKA, we used the inhibitors SQ22536 [29] and H-89 [30], respectively. As shown in Figure 8*A*, 20 μM H-89 and 100 μM SQ22536 both attenuated the high ERK1/2 activity in AT6.1 cells. At 5 minutes, p-ERK1/2 was 69 ± 5% and 74 ± 9% of control, whereas at 15 minutes it was 49 ± 6% and 53 ± 10% of control in the presence of H-89 (Figure 8*A*, *left panel*) and SQ22536 (Figure 8*A*, *middle panel*), respectively. Because protein kinase C (PKC) is a known regulator of $p47^{phox}$ activation, we determined the role of PKC in these cells by using the selective inhibitor, BIM. BIM (1 μM) did not significantly change the p-ERK1/2 levels at the two time points examined (Figure 8*A*, *right panel*).

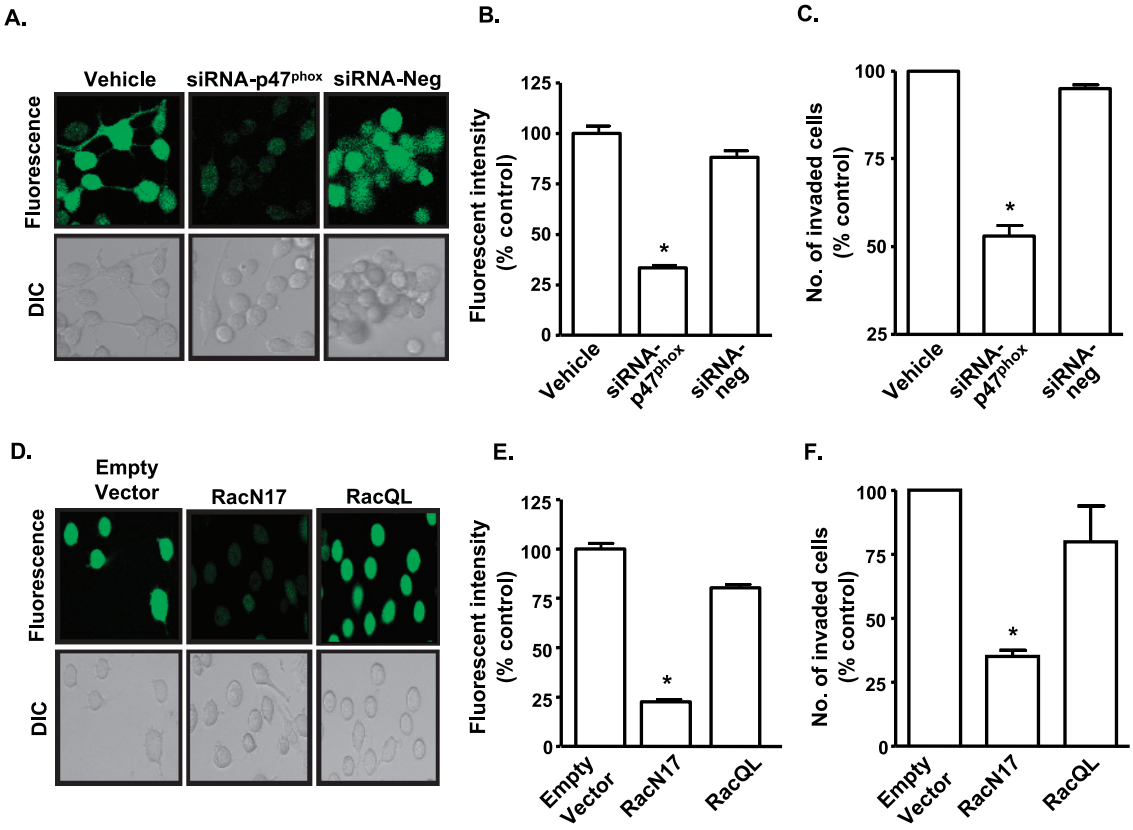

Figure 4. NADPH oxidase mediates ROS generation and invasion of AT6.1 cells. (A and B) AT6.1 cells were transfected with a siRNA against $p47^{phox}$ (siRNA-$p47^{phox}$) or scrambled-siRNA (siRNA-neg) for 72 hours (A), and ROS generation was determined by incubating the cells with H_2DCFDA. siRNA-$p47^{phox}$ suppressed ROS generation. Histograms shown in panel B represent the mean ± SEM of three separate experiments. Asterisk indicates statistically significant difference ($P < .01$) from vehicle-treated controls. (C and D) AT6.1 cells were transfected with an empty plasmid vector or an expression vector encoding the constitutively active (RacQL) or dominant-negative (RacN17) Rac1 plasmids for 24 hours. ROS generation in these cells was imaged (D) and quantitated in (E) and shows suppression of ROS in RacN17 transfectants but comparable levels of ROS, as observed in empty vector, in RacQL transfectants. Invasion chamber assays were performed in cells transfected with vehicle, siRNA-Neg, or siRNA-$p47^{phox}$ (C) or with Rac1 mutants (F). Histograms indicate the extent of Matrigel invasion from three different experiments. Inhibition of cell invasion was observed in cells treated with siRNA-$p47^{phox}$ and RacN17. Asterisk indicates statistically significant difference from control ($P < .01$).

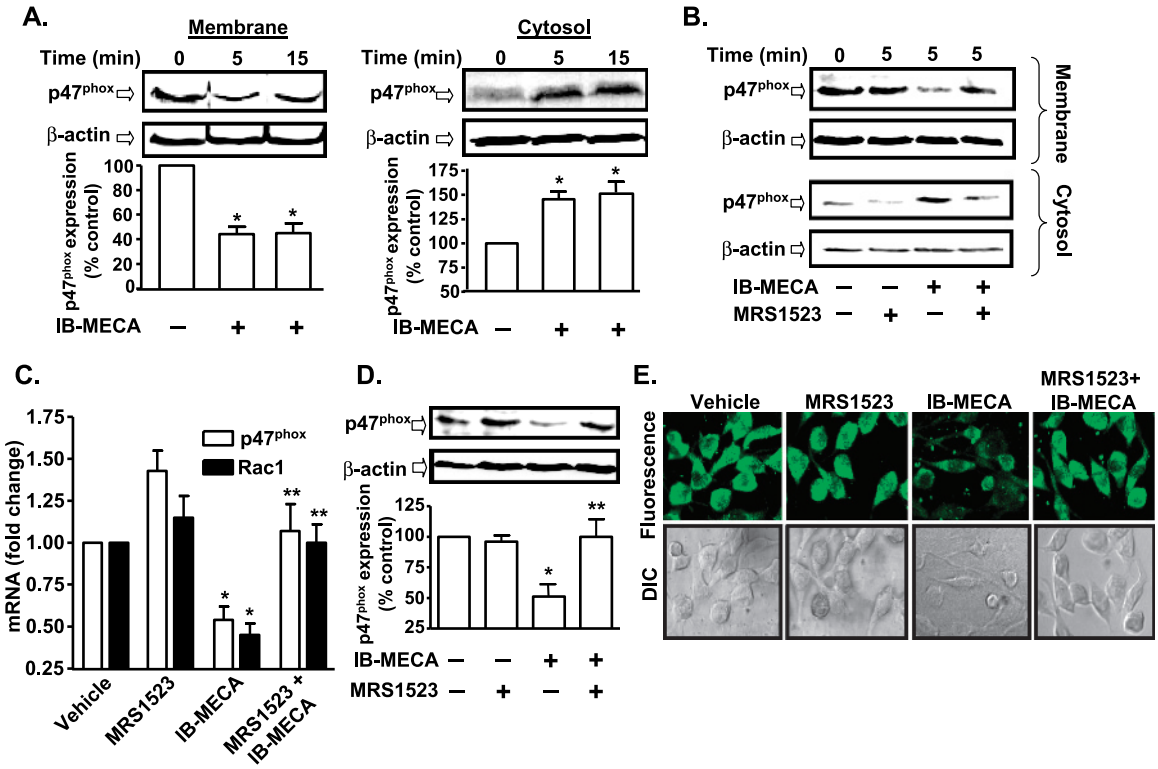

Figure 5. Inhibition of p47^{phox} activity and Rac1 expression by A_3AR activation. (A) Western blot analysis for p47^{phox} was performed in membrane and cytosolic fractions from AT6.1 cells after 1 μM IB-MECA treatment for indicated time points. Vehicle-treated cells served as controls. Blots were stripped and probed for β-actin to normalize for protein loading. The figure shows reduced membrane localization and increased cytosolic levels of p47^{phox} at 5 and 15 minutes after IB-MECA administration. Histograms represent the mean ± SEM of four different Western blot experiments quantified by Un-Scan-It software. Asterisk (*) indicates statistically significant difference ($P < .05$) from control. (B) AT6.1 cells were pretreated with MRS1523 for 30 minutes, followed by IB-MECA treatment for 5 minutes, and membrane and cytosolic isolates were obtained for p47^{phox} Western blot studies. MRS1523 reduced the ability of IB-MECA to reduce membrane localization (or increase cytosolic localization) of p47^{phox}. The blot presented is a representative from five different experiments with identical results. (C) AT6.1 cells were treated with vehicle, IB-MECA (1 μM), MRS1523 (1 μM), or MRS1523 + IB-MECA for 24 hours, and p47^{phox} and Rac1 transcripts were measured by real-time RT-PCR. Histograms indicate the mean ± SEM of the fold change in transcripts levels. (D) Levels of p47^{phox} determined by Western blot analysis. Cells were pretreated with vehicle or MRS1523 for 30 minutes followed by IB-MECA for 24 hours. IB-MECA reduced p47^{phox} levels, which was inhibited by MRS1523. Histograms indicate the mean ± SEM of at least five different experiments. Asterisks (*) and (**) represent statistically significant difference from vehicle- and IB-MECA–treated groups, respectively ($P < .05$). (E) Immunocytochemistry for Rac1 was performed on the cells grown on glass coverslips and treated with indicated reagents for 24 hours. Fluorescent and DIC images are a representation from three independent experiments performed in duplicates.

Pretreatment of AT6.1 cells with either H-89 or SQ22536 significantly reduced ROS generation, whereas PKC inhibitor BIM did not have any effect (Figure 8*B*). In addition, both H-89 and SQ22536 reduced the membrane localization of p47^{phox} (Figure 8*C*), whereas BIM showed no significant effect (Figure 8*D*). These data implicate the cyclic AMP/PKA pathway in the activation of ERK1/2 and the NADPH oxidase system. Whereas PD098059, H-89, and SQ22536 significantly suppressed invasion of AT6.1 cells to 46 ± 3%, 35 ± 5%, and 48 ± 6% of controls, respectively, BIM did not affect AT6.1 cells invasion (Figure 8*E*).

Discussion

This study demonstrates that activation of the A_3AR reduces proliferation and metastasis of prostate cancer cells both *in vitro* and *in vivo*. We have identified two major targets of the A_3AR crucial for regulating both proliferation and invasion. These are the ERK-MAP kinase pathway and NADPH oxidase, an important regulator of ROS generation in prostate cancer cells. Furthermore, ERK1/2 activity and NADPH oxidase activity in these cells seemed to be dependent on the activity of adenylyl cyclase and PKA because inhibition of both the enzymes reduced ERK1/2 activation as well as ROS generation and cell invasion.

The incidence and prevalence of prostate cancer increase with increasing age, and one of the important risk factors linked to this increased propensity is the generation of high levels of ROS in the prostate cancer cells. ROS is normally produced as part of the aerobic cellular respiration, and low to moderate levels of ROS play a critical role in the intracellular signaling pathways [31]. However, the levels of ROS within the cells become high, whereas the levels of the antioxidant enzymes are reduced with aging [32]. In the present study, we observed high levels of ROS in different prostate cancer cell lines, including the human PC3-MM and ALVA and rat AT6.1 cell lines. The high levels of ROS are believed to directly damage cellular DNA and proteins, which might further aggravate malignant transformation. A link between high ROS and prostate cancer is indirectly supported by the studies showing that antioxidants such as lycopene, vitamin E, selenium, and soy can reduce the risk of prostate cancers [33].

One of the major sources of ROS generation in the cells is the NADPH oxidase enzyme system. Previous studies have shown increased

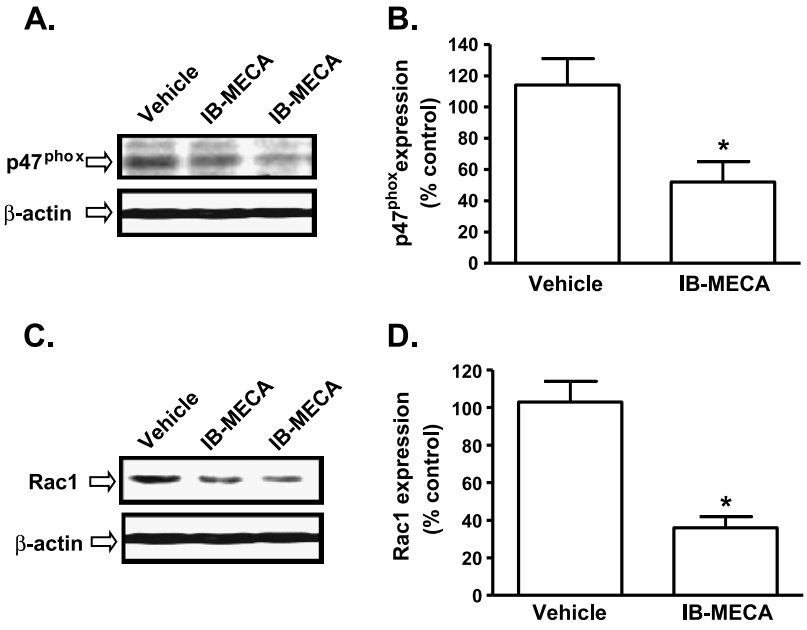

Figure 6. A_3AR agonist decreases p47^{phox} and Rac1 levels *in vivo*. SCID mice were administered AT6.1 cells by subcutaneous injections. When the tumor size was approximately 100 mm^3 (~day 9), these mice were administered vehicle or IB-MECA (10 μg/kg), and treatments were continued on alternate day up to day 33. Subcutaneous tumors were then excised and used for Western blot analysis for p47^{phox} and Rac1. (A and B) Western blots and densitometric analyses of p47^{phox} levels from four mice. (C and D) Western blots and densitometric analyses of Rac1 levels from four mice. Data are presented as the mean ± SEM of four different experiments. Asterisk (*) indicates statistically significant difference ($P < .05$) from vehicle-treated SCID mice.

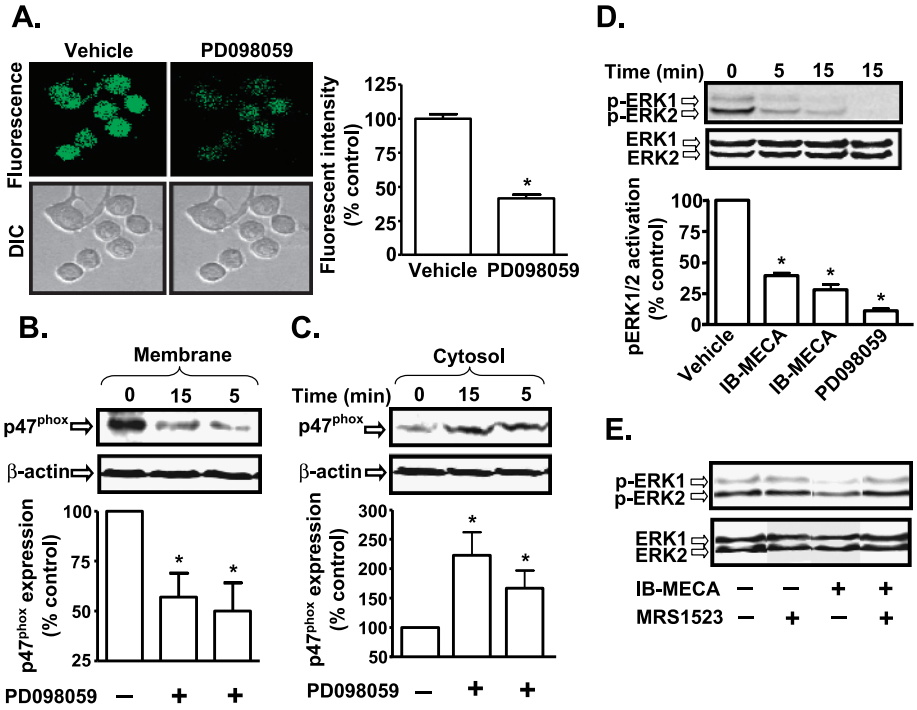

Figure 7. ERK1/2 MAP kinase regulates NADPH oxidase activity. (A) AT6.1 cells were treated with either vehicle or PD098059 (10 μM) for 15 minutes. Cells were then incubated with H_2DCFDA for 20 minutes, and ROS generation was recorded by confocal microscopy. The histograms show the levels of ROS generation and represent the mean ± SEM of three different experiments. Asterisk (*) indicates statistically significant difference from control ($P < .01$). (B and C) p47^{phox} Western blot analysis was performed on isolated membrane (B) and cytosolic (C) fractions of vehicle- or PD098059-treated cells. Representative blot shows reduced activation of p47^{phox}, indicated by reduced membrane level of p47^{phox} by PD098059. Histograms represent the mean ± SEM of five different experiments. Asterisk (*) indicates statistically significant difference ($P < .05$) from vehicle-treated control cells. (D) IB-MECA reduced ERK1/2 activation in AT6.1 cells. The Western blot image is a representative of six different experiments with similar results. Data presented in the histogram are the mean ± SEM. Asterisk (*) indicates statistically significant difference from vehicle-treated controls ($P < .01$). (E) A_3AR antagonist MRS1523 reduces inhibition of ERK1/2 phosphorylation by IB-MECA. Blot is representative of four separate experiments with identical results.

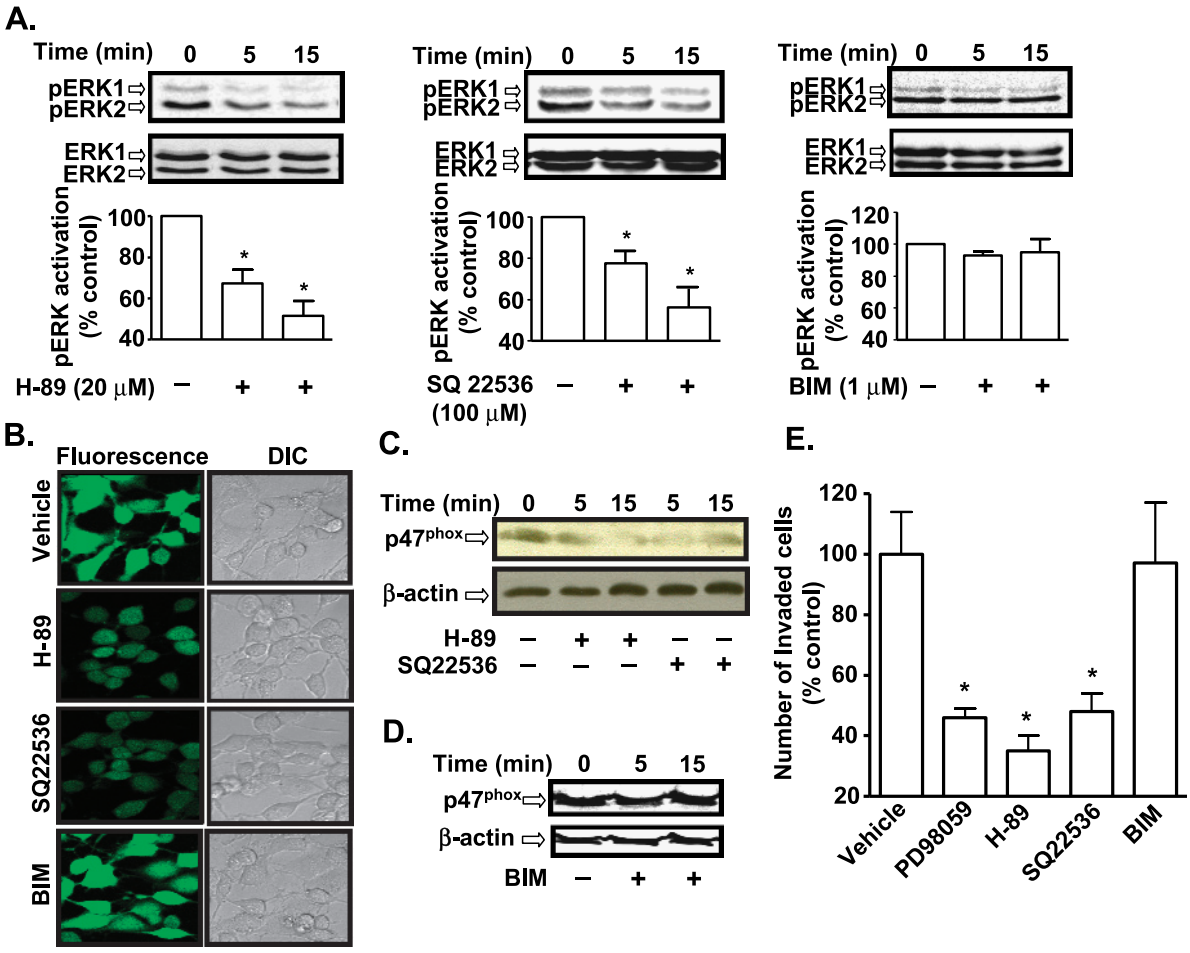

Figure 8. Inhibition of the cyclic AMP/PKA pathway abrogates ERK1/2 activity. (A) AT6.1 cells were treated with H-89 (PKA inhibitor; 20 μM), SQ22536 (adenylyl cyclase inhibitor; 100 μM) or BIM (PKC inhibitor; 1 μM) for 5 or 15 minutes. Western blot analysis was performed for p-ERK1/2 and normalized to total ERK1/2. Histograms indicate the mean ± SEM of at least five separate experiments. Asterisk (*) indicates statistically significant difference from control cells ($P < .01$). (B) AT6.1 cells were treated with H-89, SQ22536, and BIM for 15 minutes, and ROS generation was determined by measuring the fluorescence of H_2DCFDA dye. H-89 and SQ22536 decreased ROS generation, whereas BIM was without effect. (C and D) AT6.1 cells were treated with vehicle, H-89, or SQ22536 (C) or BIM (D) for 5 and 15 minutes. Western blot analysis was performed for $p47^{phox}$ on the membrane fraction. Blot shown is a representative of three separate experiments that show similar results. (E) AT6.1 cells were plated on the top chamber of the Matrigel invasion chamber and treated with vehicle, PD098059 (10 μM), H-89 (20 μM), SQ22536 (100 μM), or BIM (1 μM) for 24 hours. The number of invaded cells was determined as described in Materials and Methods and normalized as percent of vehicle-treated controls. The histogram represents the mean ± SEM of three different experiments. Asterisk (*) indicates statistically significant difference from vehicle-treated control cells ($P < .05$).

ROS in the presence of prostate-specific antigen and testosterone in both androgen-dependent (LNCaP) and -independent cell lines (PC3 and DU145) [34]. Brar et al. [35] reported the involvement of NADPH oxidase subunits, $gp91^{phox}$ and NOX5, in regulating the growth of the androgen-independent DU145 prostate cancer cells. Increased ROS generation and expression of NOX1 were also observed in human prostate cancer specimens [36] and in ovarian cancer cells where siRNA against NADPH oxidase subunits NOX4 and $p47^{phox}$ reduced the high basal ROS generation [37]. Similarly, we also observed high NADPH oxidase activity in various prostate cancer cell lines, including both androgen-dependent and -independent lines, examined in this study. The ability of chemical inhibitors such as DPI and AEBSF, as well as of siRNA against $p47^{phox}$ and dominant-negative Rac1, to inhibit ROS generation implicates NADPH oxidase as a major contributor of ROS generation in these prostate cancer cells. The antitumor action of IB-MECA seems to be linked to the inhibition of NADPH oxidase in these cells. ROS can mediate mitogenic signaling and regulate the actions of transcription factors, such as activator protein-1 and nuclear factor κB and protein kinases, such as protein kinase C and ERK1/2 MAP kinases [38]. Constitutive activation of ERK1/2 has been observed in leukemia [39], breast cancer [40], and ovarian cancer [41], where they might promote tumor metastasis in addition to cell proliferation. In melanoma cells, ERK1/2 increases the cell invasion by activating matrix metalloproteinases (MMPs) such as MMP-1, -2, and -9 [42]. Increased ERK1/2 activation has also been implicated in the increased migration of PC3 prostate cancer cells in the presence of lysophosphatidic acid [43]. These studies support the involvement of ERK1/2 in mediating both cell proliferation and metastasis.

In the present study, we show that the A_3AR inhibits ERK1/2 activity in AT6.1 cells presumably by inhibiting the activity of adenylyl cyclase through the G_i protein(s), leading to reduced cyclic AMP levels and activation of PKA. It seems that this adenylyl cyclase–PKA signaling pathway is crucial for maintaining the high basal ERK1/2 activity in these cells because inhibition of these enzymes reduced ERK1/2

activity. Activation of ERK1/2 activity by PKA is likely mediated at the level of the B-Raf protein, which seems to serve as a substrate for PKA [44]. Similar to our findings, inhibition of ERK1/2 phosphorylation by A_3AR agonist has been demonstrated in melanoma [45] and thyroid cancer cells [46]. In melanoma cells, the inhibition of ERK1/2 phosphorylation was dependent on A_3AR and phosphatidylinositol 3-kinase/Akt activation [45]. Activation of phosphatidylinositol 3-kinase/Akt pathway resulted in the phosphorylation of Raf at an inhibitory site leading to decreased ERK1/2 activation [45]. In contrast, A_3AR agonists promoted ERK1/2 activity in colon cancer cell lines [47], and A_3AR transfected Chinese hamster ovary (CHO) cells [48]. The reason for these differing responses in different cells is not clear but could relate to the levels of basal ERK1/2 activity demonstrated in these cells. For example, like prostate cancer, melanoma and thyroid cancer cells might express high ERK1/2 activity, whereas colon cancer cell lines and A_3AR-transfected CHO cells might express low ERK1/2 activity.

In our study, we found that the inhibitory effects of A_3AR agonist, IB-MECA, were suppressed by the A_3AR-specific antagonist MRS1523, supporting our hypothesis that IB-MECA–induced effects were in fact receptor-dependent. However, several studies have shown an A_3AR-independent effect of A_3AR agonist in inducing apoptosis of leukemia cells [49], breast cancer cells [50], HT-29 colon cancer cells [51], and thyroid cancer cells [46]. In general, these responses were obtained at high micromolar concentrations of the agonists, suggesting they might involve activation of different ARs or other cellular targets.

Several pieces of evidence obtained from this study suggest that the activity of NADPH oxidase is dependent on ERK1/2. For example, we show that inhibition of ERK1/2 by PD098059 reduces plasma membrane localization of $p47^{phox}$ in AT6.1 cells, a requirement for the activation of this enzyme. This was correlated with increased cytosolic levels of $p47^{phox}$. Such a pathway of ERK1/2 and $p47^{phox}$ interaction could aid in the maintenance of the high ROS generation observed in these cells. Activation of $p47^{phox}$ by ERK1/2 is well studied in human neutrophils [26,27]. The primary sequence on substrates targeted by ERK1/2 is Pro-Xaa_n-Ser/Thr-Pro, where Xaa is a neutral of basic amino acid and n = 1 or 2 [52]. Human $p47^{phox}$ possess various serine residues located in the C-terminus, which are phosphorylated during its activation [53]. Of these, Ser-345 and Ser-348 are located in target sequences recognized by ERK1/2 (–Pro–X–Ser–Pro–), where X represents a neutral or basic amino acid [53]. Rat $p47^{phox}$ also contains the ERK1/2 target sequence with serine residues at positions –346 and 349 [54], but the mouse $p47^{phox}$ C-terminus is devoid of an ERK1/2 target sequence [55]. Thus, unlike the mouse $p47^{phox}$, the human and rat $p47^{phox}$ subunits are potential targets of ERK1/2–mediated phosphorylation, as suggested by our findings.

In addition to the activation of NADPH oxidase system, ERK1/2 might also induce Rac1 activity or expression, as seen in colon cancer cells and prostate cancer cells [56,57]. The high expression of Rac1 demonstrated in our study was also observed in a recent study by Engers et al. [58], which showed high Rac1 expression in high-grade prostatic intraepithelium neoplasia and prostatic carcinoma, compared with benign secretory epithelium in human prostate tissue specimens. Thus, Rac1 and $p47^{phox}$ not only are regulators of ROS generation but also are regulated by ROS-dependent activation of the ERK1/2 pathway. In breast cancer cells and squamous cell carcinoma, Rac1 activity is stimulated by PKA, which promotes migration of these cancer cells [59]. In the current study, we demonstrated that activation of the A_3AR (which inhibits adenylyl cyclase activity and expected to decrease PKA) inhibited $p47^{phox}$ expression and prostate cancer cell invasiveness. On the basis of the above discussion, it seems reasonable to speculate that the mechanism underlying inhibition of prostate cancer cell proliferation and metastasis through the A_3AR involves suppression of an adenylyl cyclase–PKA signaling pathway, which directly regulates ERK1/2 MAP kinase and NADPH oxidase.

Whereas our study highlights the importance of controlling ROS generation in the treatment of prostate cancers, we are not able to discern any differences in A_3AR-mediated inhibition of cell proliferation and motility in androgen-dependent (such as ALVA) and androgen-independent prostate cancer lines (such as AT6.1 and PC3-MM). All of these cell lines showed relatively similar responses to IB-MECA. This suggests that IB-MECA could be useful in androgen-independent prostate cancer, in which treatment options (such as androgen withdrawal therapy) might be more limited. Furthermore, our studies did not highlight any difference in the pathways linked to proliferation *versus* metastasis. It seems that the ERK1/2 pathway might subserve both functions. ERK1/2 can promote tumor cell proliferation by controlling the activity of different cell cycle regulators, such as increasing the transcription of cyclin D1, activation of cyclin-dependent kinases or inhibition of cyclin-dependent kinase inhibitor $p27^{Kip1}$ [60]. In addition, ERK1/2 can also increase the tumor cell migration and invasion by increasing the expression of Rac1 and MMP-1, -2, and-9 [42,57]. Inhibition of ERK1/2 activity by IB-MECA could therefore suppress both prostate cancer cell proliferation and metastasis.

In summary, our data show that IB-MECA suppresses prostate cancer growth and metastasis *in vivo*. This action is believed to be mediated through suppression of the high NADPH oxidase activity in these cells by inhibiting the upstream adenylyl cyclase/PKA pathway. PKA positively regulates ERK1/2 activity, which serves as a direct activator of $p47^{phox}$ subunit of NADPH oxidase. In addition, activation of the A_3AR reduced expression of the $p47^{phox}$ and Rac1 subunits of this enzyme and thereby removes the positive feedback regulation of ROS generation in these cells. On the basis of our and other similar studies on prostate cancers, we propose that A_3AR agonists could be useful clinically in controlling the growth and metastasis of androgen-dependent and -independent prostate cancers.

Acknowledgments

The authors thank Z. Nie and P.A. Randazzo at the National Cancer Institute, National Institutes of Health, Bethesda, MD, for generously providing plasmid vectors expressing RacQL and RacN17.

References

[1] Jemal A, Siegel R, Ward E, Hao Y, Xu J, Murray T, and Thun MJ (2008). Cancer statistics 2008. *CA Cancer J Clin* **58**, 71–96.

[2] Condeelis JS, Wyckoff JB, Bailly M, Pestell R, Lawrence D, Backer J, and Segall JE (2001). Lamellipodia in invasion. *Semin Cancer Biol* **11**, 119–128.

[3] Ridley AJ, Schwartz MA, Burridge K, Firtel RA, Ginsberg MH, Borisy G, Parsons JT, and Horwitz AR (2003). Cell migration: integrating signals from front to back. *Science* **302**, 1704–1709.

[4] Lee TK, Man K, Ho JW, Wang XH, Poon RT, Sun CK, Ng KT, Ng IO, Xu R, and Fan ST (2005). Significance of the Rac signaling pathway in HCC cell motility: implications for a new therapeutic target. *Carcinogenesis* **26**, 681–687.

[5] Bouzahzah B, Albanese C, Ahmed F, Pixley F, Lisanti MP, Segall JD, Condeelis J, Joyce D, Minden A, Der CJ, et al. (2001). Rho family GTPases regulate mammary epithelium cell growth and metastasis through distinguishable pathways. *Mol Med* **7**, 816–830.

[6] Uhlenbrock K, Eberth A, Herbrand U, Daryab N, Stege P, Meier F, Friedl P, Collard JG, and Ahmadian MR (2004). The RacGEF Tiam1 inhibits migration and invasion of metastatic melanoma via a novel adhesive mechanism. *J Cell Sci* **117**, 4863–4871.

[7] Hall A (1992). Ras-related GTPases and the cytoskeleton. *Mol Biol Cell* **3**, 475–479.
[8] Haas A and Goebel W (1992). Microbial strategies to prevent oxygen-dependent killing by phagocytes. *Free Radic Res Commun* **16**, 137–157.
[9] Bedard K and Krause KH (2007). The NOX family of ROS-generating NADPH oxidases: physiology and pathophysiology. *Physiol Rev* **87**, 245–313.
[10] Lassègue B and Clempus RE (2003). Vascular NAD(P)H oxidases: specific features, expression, and regulation. *Am J Physiol Regul Integr Comp Physiol* **285**, R277–R297.
[11] Behrend L, Henderson G, and Zwacka RM (2003). Reactive oxygen species in oncogenic transformation. *Biochem Soc Trans* **31**, 1441–1444.
[12] Karin M, Takahashi T, Kapahi P, Delhase M, Chen Y, Makris C, Rothwarf D, Baud V, Natoli G, Guido F, et al. (2001). Oxidative stress and gene expression: the AP-1 and NF-kappaB connections. *Biofactors* **15**, 87–89.
[13] Ramkumar V, Hallam DM, and Nie Z (2001). Adenosine, oxidative stress and cytoprotection. *Jpn J Pharmacol* **86**, 265–274.
[14] Tey HB, Khoo HE, and Tan CH (1992). Adenosine modulates cell growth in human epidermoid carcinoma (A431) cells. *Biochem Biophys Res Commun* **187**, 1486–1492.
[15] Colquhoun A and Newsholme EA (1997). Inhibition of human tumour cell proliferation by analogues of adenosine. *Cell Biochem Funct* **15**, 135–139.
[16] Ryzhov S, Novitskiy SV, Zaynagetdinov R, Goldstein AE, Carbone DP, Biaggioni I, Dikov MM, and Feoktistov I (2008). Host A(2B) adenosine receptors promote carcinoma growth. *Neoplasia* **10**, 987–995.
[17] Madi L, Bar-Yehuda S, Barer F, Ardon E, Ochaion A, and Fishman P (2003). A_3 adenosine receptor activation in melanoma cells: association between receptor fate and tumor growth inhibition. *J Biol Chem* **278**, 42121–42130.
[18] Ohana G, Bar-Yehuda S, Arich A, Madi L, Dreznick Z, Rath-Wolfson L, Silberman D, Slosman G, and Fishman P (2003). Inhibition of primary colon carcinoma growth and liver metastasis by the A_3 adenosine receptor agonist CF101. *Br J Cancer* **89**, 1552–1558.
[19] Fishman P, Bar-Yehuda S, Ardon E, Rath-Wolfson L, Barrer F, Ochaion A, and Madi L (2003). Targeting the A_3 adenosine receptor for cancer therapy: inhibition of prostate carcinoma cell growth by A_3AR agonist. *Anticancer Res* **23**, 2077–2083.
[20] Fishman P, Bar-Yehuda S, Ohana G, Barer F, Ochaion A, Erlanger A, and Madi L (2004). An agonist to the A_3 adenosine receptor inhibits colon carcinoma growth in mice via modulation of GSK-3 beta and NF-kappa B. *Oncogene* **23**, 2465–2471.
[21] Madi L, Ochaion A, Rath-Wolfson L, Bar-Yehuda S, Erlanger A, Ohana G, Harish A, Merimski O, Barer F, and Fishman P (2004). The A_3 adenosine receptor is highly expressed in tumor *versus* normal cells: potential target for tumor growth inhibition. *Clin Cancer Res* **10**, 4472–4479.
[22] Merighi S, Benini A, Mirandola P, Gessi S, Varani K, Simioni C, Leung E, Maclennan S, Baraldi PG, and Borea PA (2007). Caffeine inhibits adenosine-induced accumulation of hypoxia-inducible factor-1α, vascular endothelial growth factor, and interleukin-8 expression in hypoxic human colon cancer cells. *Mol Pharmacol* **72**, 395–406.
[23] Gessi S, Cattabriga E, Avitabile A, Gafa' R, Lanza G, Cavazzini L, Bianchi N, Gambari R, Feo C, Liboni A, et al. (2004). Elevated expression of A_3 adenosine receptors in human colorectal cancer is reflected in peripheral blood cells. *Clin Cancer Res* **10**, 5895–5901.
[24] Jajoo S, Mukherjea D, Pingle S, Sekino Y, and Ramkumar V (2006). Induction of adenosine A_1 receptor expression by pertussis toxin via an adenosine 5′-diphosphate ribosylation–independent pathway. *J Pharmacol Exp Ther* **317**, 1–10.
[25] Puntambekar P, Mukherjea D, Jajoo S, and Ramkumar V (2005). Essential role of Rac1/NADPH oxidase in nerve growth factor induction of TRPV1 expression. *J Neurochem* **95**, 1689–1703.
[26] Dewas C, Fay M, Gougerot-Pocidalo MA, and El-Benna J (2000). The mitogen-activated protein kinase extracellular signal–regulated kinase 1/2 pathway is involved in formyl-methionyl-leucyl-phenylalanine–induced p47phox phosphorylation in human neutrophils. *J Immunol* **165**, 5238–5244.
[27] Hazan-Halevy I, Levy T, Wolak T, Lubarsky I, Levy R, and Paran E (2005). Stimulation of NADPH oxidase by angiotensin II in human neutrophils is mediated by ERK, p38 MAP-kinase and cytosolic phospholipase A_2. *J Hypertens* **23**, 1183–1190.
[28] Fredholm BB, Arslan G, Halldner L, Kull B, Schulte G, and Wasserman W (2000). Structure and function of adenosine receptors and their genes. *Naunyn Schmiedebergs Arch Pharmacol* **362**, 364–374.
[29] Haslam RJ, Davidson MM, and Desjardins JV (1978). Inhibition of adenylate cyclase by adenosine analogues in preparations of broken and intact human platelets. Evidence for the unidirectional control of platelet function by cyclic AMP. *Biochem J* **176**, 83–95.
[30] Chijiwa T, Mishima A, Hagiwara M, Sano M, Hayashi K, Inoue T, Naito K, Toshioka T, and Hidaka H (1990). Inhibition of forskolin-induced neurite outgrowth and protein phosphorylation by a newly synthesized selective inhibitor of cyclic AMP–dependent protein kinase, *N*-[2-(*p*-bromocinnamylamino)ethyl]-5-isoquinolinesulfonamide (H-89), of PC12D pheochromocytoma cells. *J Biol Chem* **265**, 5267–5272.
[31] Dröge W (2002). Free radicals in the physiological control of cell function. *Physiol Rev* **82**, 47–95.
[32] Ripple MO, Henry WF, Rago RP, and Wilding G (1997). Prooxidant-antioxidant shift induced by androgen treatment of human prostate carcinoma cells. *J Natl Cancer Inst* **89**, 40–48.
[33] Nelson WG, De Marzo AM, and Isaacs WB (2003). Prostate cancer. *N Engl J Med* **349**, 366–381.
[34] Sun XY, Donald SP, and Phang JM (2001). Testosterone and prostate specific antigen stimulate generation of reactive oxygen species in prostate cancer cells. *Carcinogenesis* **22**, 1775–1780.
[35] Brar SS, Corbin Z, Kennedy TP, Hemendinger R, Thornton L, Bommarius B, Arnold RS, Whorton AR, Sturrock AB, Huecksteadt TP, et al. (2003). NOX5 NAD(P)H oxidase regulates growth and apoptosis in DU 145 prostate cancer cells. *Am J Physiol Cell Physiol* **285**, C353–C369.
[36] Lim SD, Sun C, Lambeth JD, Marshall F, Amin M, Chung L, Petros JA, and Arnold RS (2005). Increased Nox1 and hydrogen peroxide in prostate cancer. *Prostate* **62**, 200–207.
[37] Xia C, Meng Q, Liu LZ, Rojanasakul Y, Wang XR, and Jiang BH (2007). Reactive oxygen species regulate angiogenesis and tumor growth through vascular endothelial growth factor. *Cancer Res* **67**, 10823–10830.
[38] Martindale JL and Holbrook NJ (2002). Cellular response to oxidative stress: signaling for suicide and survival. *J Cell Physiol* **192**, 1–15.
[39] Towatari M, Iida H, Tanimoto M, Iwata H, Hamaguchi M, and Saito H (1997). Constitutive activation of mitogen-activated protein kinase pathway in acute leukemia cells. *Leukemia* **11**, 479–484.
[40] Sivaraman VS, Wang H, Nuovo GJ, and Malbon CC (1997). Hyperexpression of mitogen-activated protein kinase in human breast cancer. *J Clin Invest* **99**, 1478–1483.
[41] Steinmetz R, Wagoner HA, Zeng P, Hammond JR, Hannon TS, Meyers JL, and Pescovitz OH (2004). Mechanisms regulating the constitutive activation of the extracellular signal–regulated kinase (ERK) signaling pathway in ovarian cancer and the effect of ribonucleic acid interference for ERK1/2 on cancer cell proliferation. *Mol Endocrinol* **18**, 2570–2582.
[42] Tsubaki M, Matsuoka H, Yamamoto C, Kato C, Ogaki M, Satou T, Itoh T, Kusunoki T, Tanimori Y, and Nishida S (2007). The protein kinase C inhibitor, H7, inhibits tumor cell invasion and metastasis in mouse melanoma via suppression of ERK1/2. *Clin Exp Metastasis* **24**, 431–438.
[43] Hao F, Tan M, Xu X, Han J, Miller DD, Tigyi G, and Cui MZ (2007). Lysophosphatidic acid induces prostate cancer PC3 cell migration via activation of LPA(1), p42 and p38α. *Biochim Biophys Acta* **1771**, 883–892.
[44] Calipel A, Mouriaux F, Glotin AL, Malecaze F, Faussat AM, and Mascarelli F (2006). Extracellular signal–regulated kinase–dependent proliferation is mediated through the protein kinase A/B–Raf pathway in human uveal melanoma cells. *J Biol Chem* **281**, 9238–9250.
[45] Merighi S, Benini A, Mirandola P, Gessi S, Varani K, Leung E, Maclennan S, and Borea PA (2005). A_3 adenosine receptor activation inhibits cell proliferation via phosphatidylinositol 3-kinase/Akt–dependent inhibition of the extracellular signal–regulated kinase 1/2 phosphorylation in A375 human melanoma cells. *J Biol Chem* **280**, 19516–19526.
[46] Morello S, Petrella A, Festa M, Popolo A, Monaco M, Vuttariello E, Chiappetta G, Parente L, and Pinto A (2007). Cl-IB-MECA inhibits human thyroid cancer cell proliferation independently of A_3 adenosine receptor activation. *Cancer Biol Ther* **7**, 278–284.
[47] Gessi S, Merighi S, Varani K, Cattabriga E, Benini A, Mirandola P, Leung E, MacLennan S, Feo C, Baraldi S, et al. (2007). Adenosine receptors in colon carcinoma tissues and colon tumoral cell lines: focus on the A(3) adenosine subtype. *J Cell Physiol* **211**, 826–836.
[48] Schulte G and Fredholm BB (2002). Signaling pathway from the human adenosine A(3) receptor expressed in Chinese hamster ovary cells to the extracellular signal–regulated kinase 1/2. *Mol Pharmacol* **62**, 1137–1146.

[49] Kim SG, Ravi G, Hoffmann C, Jung YJ, Kim M, Chen A, and Jacobson KA (2002). p53-Independent induction of Fas and apoptosis in leukemic cells by an adenosine derivative, Cl-IB-MECA. *Biochem Pharmacol* **63**, 871–880.

[50] Lu J, Pierron A, and Ravid K (2003). An adenosine analogue, IB-MECA, downregulates estrogen receptor alpha and suppresses human breast cancer cell proliferation. *Cancer Res* **63**, 6413–6423.

[51] Tan EY, Richard CL, Zhang H, Hoskin DW, and Blay J (2006). Adenosine downregulates DPPIV on HT-29 colon cancer cells by stimulating protein tyrosine phosphatase(s) and reducing ERK1/2 activity via a novel pathway. *Am J Physiol Cell Physiol* **291**, C433–C444.

[52] Gonzalez FA, Raden DL, and Davis RJ (1991). Identification of substrate recognition determinants for human ERK1 and ERK2 protein kinase. *J Biol Chem* **266**, 22159–22163.

[53] el Benna J, Faust LP, and Babior BM (1994). The phosphorylation of the respiratory burst oxidase component $p47^{phox}$ during neutrophil activation. Phosphorylation of sites recognized by protein kinase C and by proline-directed kinases. *J Biol Chem* **269**, 23431–23436.

[54] Tanabe M, Rådmark O, Watanabe T, Shiose A, and Sumimoto H (2005). Cloning of rat $p47^{phox}$ and comparison with human $p47^{phox}$. *DNA Seq* **16**, 65–68.

[55] Mizuki K, Kadomatsu K, Hata K, Ito T, Fan QW, Kage Y, Fukumaki Y, Sakaki Y, Takeshige K, and Sumimoto H (1998). Functional modules and expression of mouse p40(phox) and p67(phox), SH3-domain–containing proteins involved in the phagocyte NADPH oxidase complex. *Eur J Biochem* **251**, 573–582.

[56] Grijelmo C, Rodrigue C, Svrcek M, Bruyneel E, Hendrix A, de Wever O, and Gespach C (2007). Proinvasive activity of BMP-7 through SMAD4/src–independent and ERK/Rac/JNK–dependent signaling pathways in colon cancer cells. *Cell Signal* **19**, 1722–1732.

[57] Lyons LS, Rao S, Balkan W, Faysal J, Maiorino CA, and Burnstein KL (2008). Ligand-independent activation of androgen receptors by Rho GTPase signaling in prostate cancer. *Mol Endocrinol* **22**, 597–608.

[58] Engers R, Ziegler S, Mueller M, Walter A, Willers R, and Gabbert HE (2007). Prognostic relevance of increased Rac GTPase expression in prostate carcinomas. *Endocr Relat Cancer* **14**, 245–256.

[59] O'Connor KL and Mercurio AM (2001). Protein kinase A regulates Rac and is required for the growth factor–stimulated migration of carcinoma cells. *J Biol Chem* **276**, 47895–47900.

[60] Katz M, Amit I, and Yarden Y (2007). Regulation of MAPKs by growth factors and receptor tyrosine kinases. *Biochim Biophys Acta* **1773**, 1161–1176.

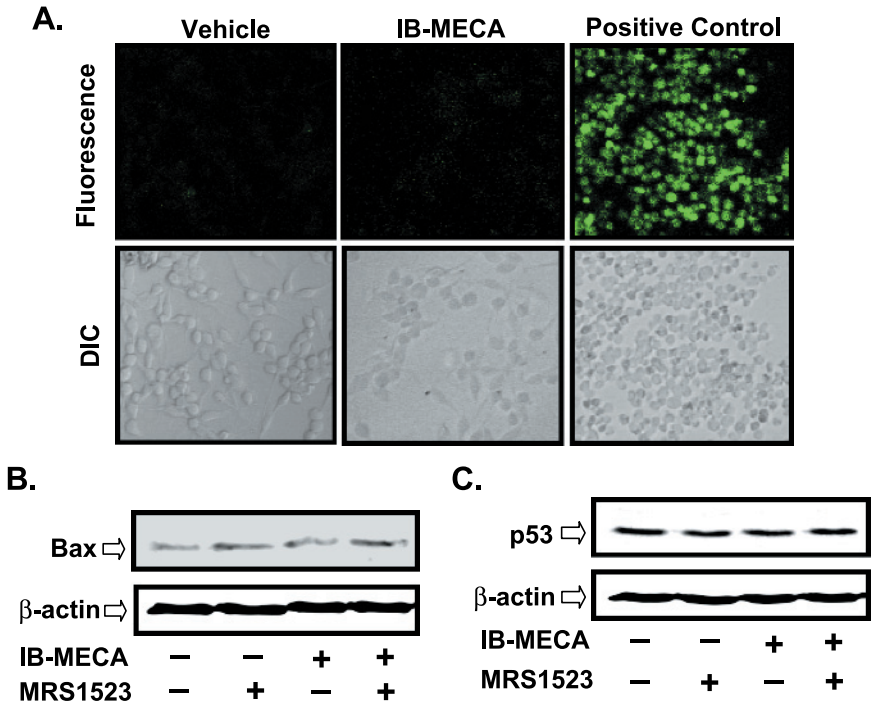

Figure W1. IB-MECA does not induce apoptosis of AT6.1 cells. (A) AT6.1 cells were cultured on glass coverslips and treated with vehicle, IB-MECA, or actinomycin D (positive control) for 24 hours. Apoptotic cell death was assessed by TUNEL assays and detected as those emitting bright green fluorescence. No significant apoptotic cells were detected in vehicle or IB-MECA–treated cultures. (B and C) Western blot analysis experiments were performed on whole-cell lysates and probed for proapoptotic proteins Bax (B) and p53 (C). No difference in Bax or p53 was observed with IB-MECA. The data presented in panels A, B, and C were replicated at least three different times and showed similar results.

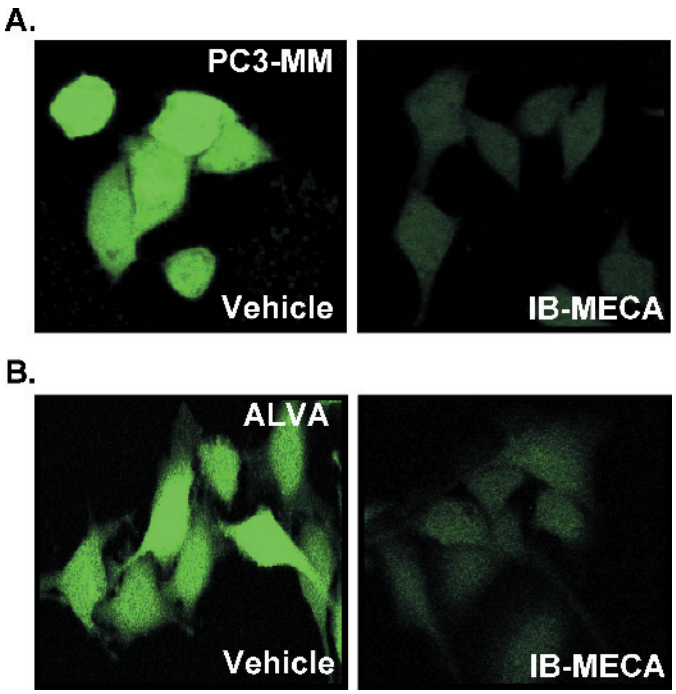

Figure W2. IB-MECA inhibits high ROS generation in PC3-MM and ALVA prostate cancer cells. PC3-MM (A) and ALVA (B) cells were cultured on glass coverslips, treated with vehicle or IB-MECA (1 μM) for 15 minutes, then incubated with H_2DCFDA for 20 minutes. ROS generation was reduced by IB-MECA in both cell lines. The data presented in panels A and B were replicated at least three different times and showed similar results.

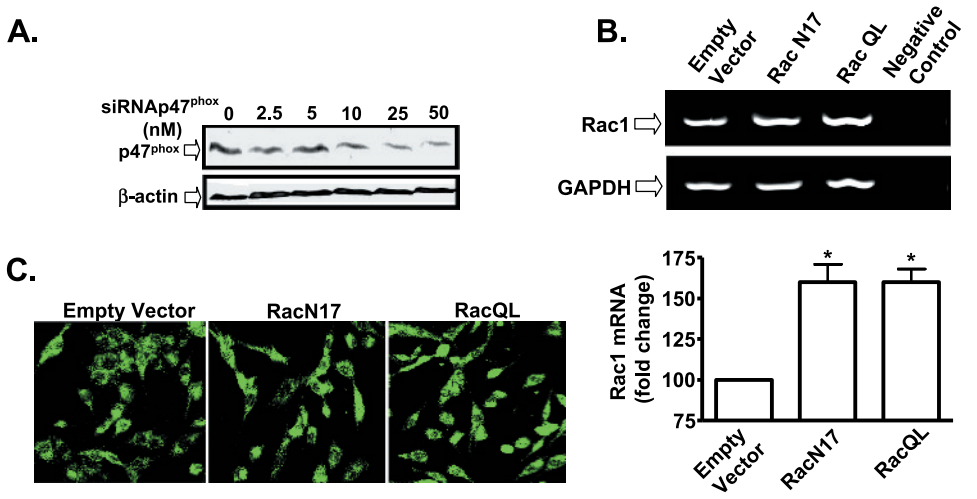

Figure W3. Inhibition of p47^{phox} (by siRNA) and Rac1 subunits (by RacN17) of NADPH oxidase in AT6.1 cells. (A) AT6.1 cells were transfected with indicated doses of scrambled siRNA (0) or p47^{phox} siRNA for 72 hours, and Western blot experiments were performed for p47^{phox} on whole cell lysates. (B) AT6.1 cells were transfected with empty vector, Rac1 dominant-negative plasmid (RacN17), or Rac1 constitutively active plasmid (RacQL), and Rac1 expression was determined by RT-PCR. Increased Rac1 expression was observed in both the RacN17 and RacQL transfectants compared with an empty vector. (C) Immunocytochemistry for Rac1 in Rac transfectants were performed and visualized by confocal microscopy. Immunolabeling was increased in RacN17 and RacQL transfectants compared with cells transfected with empty vector. The data presented in panels A, B, and C were repeated at least three times and show similar results.

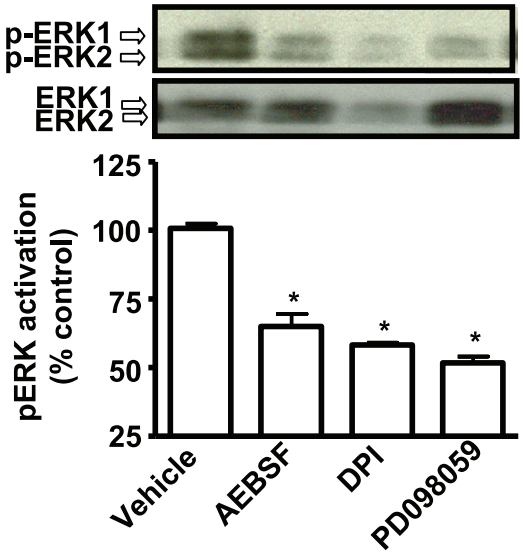

Figure W4. ROS-dependent activation of ERK1/2. AT6.1 cells were treated with vehicle, PD098059, DPI, or AEBSF for 24 hours, solubilized, and used for detection of p-ERK1/2 by Western blot analysis. Membranes were stripped and reprobed for ERK1/2 to normalize for protein loading. The blot is a representative of four different experiments with identical results. The histogram represents the normalized p-ERK1/2 data, which are presented as the mean ± SEM of four different experiments. Asterisk (*) indicates statistically significant difference ($P < .01$) from vehicle-treated control cells.

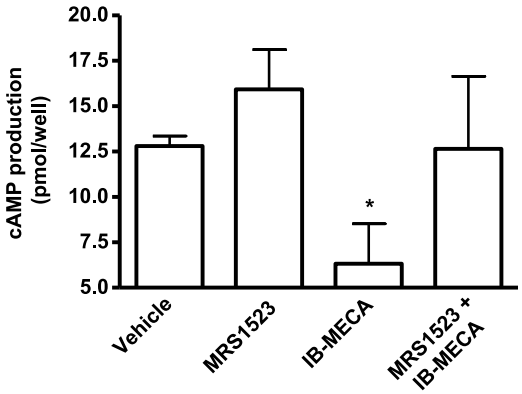

Figure W5. A_3AR activation reduces cyclic AMP (cAMP) levels in AT6.1 cells. AT6.1 cells were pretreated with vehicle or MRS1523 (1 μM) for 30 minutes, followed by 5 minutes of IB-MECA (1 μM) treatment. The cyclic AMP levels per culture well were then determined using a chemiluminescence-based cyclic AMP immunoassay kit. Histogram represents mean ± SEM of three separate experiments performed in quadruplates. Asterisk (*) indicates statistically significant difference from vehicle-treated controls ($P < .05$).

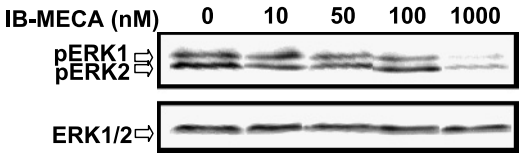

Figure W6. Dose-dependent suppression of ERK1/2 activation by IB-MECA. AT6.1 cells were treated with different doses of IB-MECA (0-1000 nM) for 15 minutes, and Western blot analysis was performed on whole cell lysates for p-ERK1/2. Normalization of the blots was done with ERK1/2. The blot represents the identical results from three separate experiments.